Application feasibility of high-performance-type plasma jet device to various material processes

Katashi Osaki, Satoru Fujimoto, Osamu Fukumasa

Department of Electrical and Electronic Engineering,
Faculty of Engineering, Yamaguchi University,
Tokiwadai 2-16-1, Ube 755-8611, Japan

Abstract

A newly designed high-performance-type plasma jet device for processing has been developed. This device can generate a high temperature and clean plasma jet and inject the process material into the center of the arc column. In order to demonstrate the application feasibility of this device to thermal processing, the effects of nozzle diameter and material loading on the characteristics of the arc and plasma jet were studied. On increasing the nozzle diameter, the jet power decreases by 0.5-1 kW but the stable device proposed would be very useful for various material processes.

Key words: plasma jet, arc plasma, plasma jet generator, plasma spray gun, plasma diagnostics

1. Introduction

Plasma jet, i.e. a thermal plasma flow, is widely used to produce new materials such as ultra-fine particles, functionally graded coatings [1] and so on. In order to obtain high-quality products, it is necessary to develop a plasma jet generator with excellent performance, i.e. a stable and clean plasma jet that can be generated over a wide range of processing conditions with easily controllable parameter (temperature, velocity, etc.), and to make clear the interaction between the plasma and the material particles injected into the plasma flow.

To this end, we have developed various plasma jet generators, such as the forced constricted [2], the local wall constricted [3] and the cross electrode [4] types, and studied the application feasibility of these generators to refractory material processing [5-10]. Since the arc maintained in these generators is extended and maintained at a constant length on account of the electrically insulated constrictor ring equipped at the nozzle inlet, a stable plasma jet is generated under various operating conditions. In addition, a cascade arc discharge source for a processing plasma [11] and a TRIPLEX torch [12] have been developed using the techniques as same as ours. It has been reported that both torches were stably operated under various operating conditions and were useful devices for various processes.

It was proved that the above-mentioned cross electrode-type plasma jet generator was a useful thermal plasma source, because the plasma jet was clean and part of the arc column in the nozzle constrictor was also used for processing. Furthermore, to use the full arc column in the nozzle constrictor for processing, we have developed a plasma electrode-type plasma jet generator. We also clarified the configuration of the electrode chamber and the flow pattern of the working gas for the arc to achieve stabilization of a U-shaped arc ignited in the nozzle constrictor [14]. Thus, we have developed a high-performance-type of plasma jet device [15] consisting of this generator and a feed pipe. To determine the application feasibility of this device to thermal processing, we studied the dependence of the performance characteristics on various operating conditions [16, 17] and the interaction between the plasma and powder particles. In addition, the velocity and size of the in-flight material particles were measured [18] using the light pulse analysis method [19].

In the present paper, the aim was to expand the operating region and clarified the

applicability of the newly designed high-performance-type plasma jet device to various material processes. Thus, we investigated the effect of the nozzle diameter and material loading on the characteristics of the arc and jet.

2. Experimental apparatus

A schematic diagram of the newly designed high-performance-type plasma jet for processing is shown in Fig.1. This device consists of a plasma electrode-type plasma jet generator and a feed pipe on the nozzle axis. The plasma jet generator constituted from a Cu rod anode of 5 mm in diameter, a rod cathode (2% Th-W) of 5 mm in diameter and a Cu nozzle of 57 mm in length. The anode and cathode are set up in each electrode chamber and installed perpendicular in the nozzle constrictor, as shown in Fig. 1, with the distance between them 39 mm. Thus, the electrode spots are separated from the nozzle constrictor section and the arc ignited between the electrodes exhibits a U-shape.

The brass feed pipe was of two types: a single pipe of 1.5-mm inner diameter for powder loading and a double pipe, with outer pipe 1.5 mm in inner diameter and the inner pipe (0.15 mm thickness) 0.5 mm in inner diameter for liquid loading.

Four kinds of nozzles were used: a P-5 nozzle with a 5-mm diameter; a P-6 nozzle with a 6-mm diameter; a P-8 nozzle with an 8-mm diameter; and an R-8 nozzle installed in the local constricting ring (Cu, 6-mm inner diameter, 8-mm outer diameter and 2/1 inlet taper) on the cathode side of the P-8 nozzle.

Experiments were carried out under the following conditions: working gas flow rate Q, 20-50 l/min; electrode sheath gas flow rate, 10 l/min; arc current I_a, 60-140 A; carrier gas flow rate Q_f for powder material (Ti, particle size 5-45 μm), 5-10 l/min; Ti feed rate, 0.5 g/min; atomizing gas flow rate Q_a for liquid material (C_2H_5OH), 7 l/min; and C_2H_5OH feed rate, 1 g/min. The gas used was argon. The DC power source was a silicon-type three-phase rectifier equipped with a ripple filter, with ratings as follows: output voltage, 200V; ripple percentage, < 0.5%; and maximum output current, 300 A.

3. Experimental results and discussion

3.1. Dependence of performance characteristics on nozzle diameter

Fig. 2 shows the relationship between the arc voltage V_a and arc current I_a for various nozzles. V_a increases linearly with increasing I_a, i.e. the V_a-I_a characteristics for the U-shaped arc show an increasing trend for all nozzles, because the length of U-shaped arc and the electric conductivity are almost constant. With increasing nozzle diameter, although both V_a and the increasing ratio of V_a decrease, the upper limit of I_a for stable operation increases. In the case of the same nozzle diameter, with a local constricting ring installed, V_a increases and the upper limit of I_a for stable operation increases further. For example, the upper limit of the arc current for stable operation with P-5, P-8 and R-8 nozzles is 100, 120 and 140 A, respectively. From, these results, it is found that the stable operating region expands by enlarging the nozzle diameter and by locally constricting the U-shaped arc.

The dependence of the heat loss for the electrodes and nozzle on I_a is shown in Fig. 3. The heat loss for the anode and cathode is 0.5-1.2 and 0.15-0.85 kW, respectively, and does not depend on the nozzle diameter. On the other hand, the heat loss for the nozzle is greater than that for the electrodes, i.e. 1-3.2 kW, and decreases with increasing nozzle diameter. In the case of the same nozzle diameter, with a local constricting ring installed, the increase in this loss is small, i.e. 0.2-0.3 kW. Furthermore, the heat loss for the electrodes and nozzle increases linearly with increasing I_a.

Fig. 4 shows the relationship between the jet power W_j –i.e. subtract heat losses for the electrodes and nozzle from the arc power, which is the product of V_a and I_a –and I_a . With increasing I_a, W_j also increases linearly, i.e. from 3.4 to 12 kW, similar to the V_a–I_a characteristics shown in Fig. 2. Thus, with increasing nozzle diameter, W_j decreases because of the decrease in V_a. For example, W_j for the R-8 nozzle is greater than that for the P-8 nozzle by 0.7-1.2 kW, because V_a for R-8 is higher and its heat loss is also greater than that for P-8. Furthermore, W_j for the R-8 nozzle is greater than that for conventional plasma jet generator.

The thermal efficiency of these nozzles is 65-72% and that of the R-8 nozzle is highest, i.e. 67-72%. Furthermore, this efficiency is higher than the thermal efficiency of a conventional nozzle by approximately 10%.

Thus, we have confirmed that the jet power is effectively controlled by the arc current and that the local constricting ring is useful in increasing the jet power and improving the thermal

efficiency.

Fig. 5 shows a typical temperature field for the U-shaped arc in the nozzle cross-section, with experimental conditions as follows: nozzle type, P-8, I_a = 100 A and Q = 50 l/min. These temperatures were measured from the backside of this device by replacing the feed pipe section with the viewing window for a CCD camera equipped with and IR interference filter (transmitted peak wave: 965 nm). The isothermal line exhibits a shape similar to a round-bottomed flask to include the cathode side of the arc column. However, it is estimated that the isothermal profile in the main arc column cross-section is a coaxial circle about the arc center axis. The temperature at the arc center axis in the P-8 nozzle is 7500-17000 K and increases with increasing I_a. For the R-8 nozzle, this value is higher by approximately 4000 K. This result confirms that the newly designed plasma jet generator with a P-8 or R-8 nozzle produced a high-temperature arc and plasma jet over a wide range of operating concitions.

3.2. Performance characteristics with process material loading

As described above, it was found that the U-shaped arc and the plasma jet were stable over a wide range of operating conditions using nozzle of large diameter, i.e. the P-8 and R-8 nozzles. Thus, the experiments described below are carried out with P-8 and R-8 nozzles, with P-8 used for liquid (C_2H_5OH) loading and R-8 for powder (Ti) loading.

The arc voltage V_a-arc current I_a characteristics during material loading, as shown in Fig. 6, show an increasing trend. During material loading, V_a increases by approximately 2% for Ti and 16% for C_2H_5OH loading. For reason, it is though that process material and the carrier or atomizing gas introduced into the present device behave as the working fluid, and the thermal pinch effect on the arc increases.

Whether process material is injected or not, the fluctuation in V_a always shows a random oscillation mode, as shown in Fig.7. However, the ratio of the fluctuation level to the mean value of V_a ranges from 0.6 to 8 % for Ti powder loading a from 16 to 20 % for C_2H_5OH loading, and this oscillation is continuous. Therefore, the arc and plasma jet of the present device are stable during processing.

Fig. 8 shows the relationship between the jet power W_j and I_a during loading of process material. With increasing I_a, W_j also increases linearly, i.e. from 3.7 to 12.8 kW. Ti powder

loading produces very little change in W_j. On the other hand, the jet power increases by approximately 1 kW during C_2H_5OH loading.

The thermal efficiency of this spray gun is 62-73 % and is higher than that of a spray gun with a conventional plasma jet generator by 5-10 %.

Fig. 9 shows photographs of the plasma jet for two different conditions: (a) with Ti powder loading and (b) with C_2H_5OH loading. When the process materials are injected into the arc maintained at high temperature, as shown in Fig. 5, material particles are effectively heated and accelerated, and the ejected from the nozzle symmetrically. Thus, intense radiation from heated material particles is observed at the top of the plasma jet.

Fig. 10 shows the radial distributions of temperature T_j in the plasma jet at a distance L = 5 mm from the nozzle exit with and without Ti powder loading Experimental operating conditions were as follows: nozzle type, R-8; I_a = 100 A; Q = 50 l/min; Q_f = 10 l/min; and Ti feed flow rate, 0.5 g/min. This spectroscopic temperature was obtained by the two-line method, i.e. Ar lines at 415.9 and 696.5 nm. Whether Ti powder is injected or not, the temperature profile shows on-axis peak characteristics, and hence T_j has a maximum value at the jet center axis r = 0 mm. With powder loading, T_j at r = 0, 1.8 and 3.1 mm is 9700, 9000 and 7000 K, and T_j at each point is lower than in the case with no loading by approximately 900, 1000 and 1600 K, respectively. Therefore, the decrease in T_j in the region of $r < 1.8$ mm is slight, but in the outer region, i.e. $r > 1.8$ mm, it decreases remarkably. However, the plasma jet sustains a high temperature, i.e. above 7000 K, during processing. Thus, in the present device, Ti powder particles introduced into the nozzle are effectively heated in the region of the arc axis and then ejected from the nozzle. Detailed mechanisms of heat transfer between the plasma flow and the powder particles are now under investigation.

4. Conclusions

The performance characteristics of the newly designed high-performance-type plasma jet device for processing were examined, in particular the effect of the nozzle diameter and material loading on the characteristics of the arc and plasma jet. The results obtained in this study are as follows:

1. The stable operating region expands with increasing nozzle diameter.

2. Jet power, i.e. net arc input power, is effectively controlled by the arc current and is large, regardless of the low-current region.
3. Jet power decreases with increasing nozzle diameter. However, the temperature of the center region of the arc is sustained at 7500-17000 K.
4. The process materials introduced into the nozzle are efficiently heated in the arc and then symmetrically ejected from the nozzle.
5. Injection of the process materials into the arc results in a drop in jet temperature of approximately 1000 K. However, the jet temperature is sustained at over 6500 K.
6. The high-performance-type plasma jet device proposed would be a very useful device for processing.

References

[1] S. Kitaguchi, N. Shimoda, T. Saito, H. Takikawa, M. Koga, J. Jpn. Soc. Powder Powder Met. 37 (1990) 918, in Japanese.

[2] K. Osaki, O. Fukumasa, A. Kobayashi, N. Tada, Appl. Plasma Sci. 4 (1996) 28, in Japanese.

[3] S. Saeki, K. Osaki, O. Fukumasa, Proceedings of the 8th International Symposium on Plasma Chemistry, Tokyo, Japan, vol. 4, 1987, p. 2259.

[4] K. Osaki, O. Fukumasa, S. Saeki, Proceedings of the 3rd Symposium on Beam Engineering Advanced Material Syntheses, Tokyo, Japan, 1992, p. 171, in Japanese.

[5] O. Fukumasa, S. Sakiyama, Trans. IEE Jpn. A 112 (1992) 269, in Japanese.

[6] S. Sakiyama, T. Hirabaru, O. Fukumasa, Rev. Sci. Instrum. 63 (1992) 2408.

[7] O. Fukumasa, Thin Solid Films 390 (2001) 37.

[8] S. Saeki, O. Fukumasa and K. Osaki, Proceedings of the 8th International Symposium on Plasma Chemistry, Tokyo, Japan, vol. 4, 1987, p. 1989.

[9] K. Osaki, O. Fukumasa, N. Tada, S. Saeki, Proceedings of the 4th Symposium on Beam Engineering Advanced Material Syntheses, Tokyo, Japan, 1993, p.11, in Japanese.

[10] K. Osaki, M. Ikuta O. Fukumasa, N. Tada, S. Saeki, Proceedings of the 5th Symposium on Beam Engineering Advanced Material Syntheses, Tokyo, Japan, 1994, p.77, in Japanese.

[11] H. Okuno, S. Yagura, H. Ishikura, H. Fujita, Rev. Sci. Instrum. 64 (1993) 990.

[12] G. Barbezat, K. Landes, Them. Spray Surf. Eng. Appl. Res. (2000) 881.

[13] K. Osaki, M. Ikuta O. Fukumasa, N. Tada, S. Saeki, Proceedings of the 6th Symposium on Beam Engineering Advanced Material Syntheses, Tokyo, Japan, 1995, p.27, in Japanese.

[14] K. Osaki, H. Ashida, N. Tada, O. Fukumasa, Mem. Fac. Eng. Yamaguchi Univ. 46 (1995) 111, in Japanese.

[15] K. Osaki, H. Ashida, N. Tada, O. Fukumasa, N. Tada, A. Kobayashi, Proceedings of ISAPS '97, Advances in Applied Plasma Science, 1997, p.61.

[16] K. Osaki, S. Fujimoto, O. Fukumasa, A. Kobayashi, Appl. Plasma Sci. 9 (2001) 43, in

Japanese.

[17] K. Osaki, S. Fujimoto, O. Fukumasa, Plasma Research Meeting in IEEJ, PST-01, 2001, p.91, in Japanese.

[18] K. Osaki, Plasma Appl. Hybrid Funct. Mater. 9 (2000) 43, in Japanese.

[19] T. Sakuta, M. I. Boulos, Rev. Sci. Instrum. 59 (1998) 289

Figure Captions

Fig. 1. Sectional view of the high-performance-type plasma jet device for processing.

Fig. 2. Arc voltage vs. arc current for various nozzles, where Q is the working gas flow rate (l/min).

Fig. 3 Heat loss for the electrodes and nozzle vs. arc current for various nozzles, where Q is the working gas flow rate (l/min).

Fig. 4 Jet power vs. arc current for various nozzles, where Q is the working gas flow rate (l/min).

Fig. 5 Temperature field of the U-shaped arc in the nozzle cross section without process material loading. These temperatures were measured using a CCD camera equipped with an IR interference filter. Experimental conditions were as follows: nozzle type, P-8; I_a = 100 A; and Q = 50 l/min.

Fig. 6 Arc voltage vs. arc current with process material loading. Experimental conditions were as follows: Q = 50 l/min; Ti feed rate, 0.5 g/min; Q_f = 5 l/min; C_2H_5OH feed rate, 1 g/min; and Q_a = 7 l/min.

Fig. 7 Oscillograms of arc voltage with and without process material loading, where M_f is the process material feed rate (g/min), Q_f is the feed gas flow rate (l/min) and Q_a is the atomizing gas flow rate (l/min). Experimental conditions were as follows: I_a = 100 A; Q = 50 l/min for (a, b) R-8 nozzle and (c) P-8 nozzle. Time scale: (a, b) 0.5 ms/division; (c) 1 ms/division. Gain: (a, b) 10 V/division; (c) 20 V/division

Fig. 8 Jet power vs. arc current during processing. Experimental conditions were as follows: Q = 50 l/min; Ti feed rate, 0.5 g/min; Q_f = 5 l/min; C_2H_5OH feed rate, 1 g/min; and Q_a = 7

l/min.

Fig. 9 Photographs of the plasma jet with process material loading, where M_f is the process material feed rate, Q_f is the feed gas flow rate (l/min) and Q_a is the atomizing gas flow rate (l/min). Experimental conditions were as follows: I_a = 100 A and Q = 50 l/min.

Fig. 10 Radial distributions of the spectroscopic jet temperature with and without Ti powder loading. Experimental conditions were as follows: I_a = 100 A; Q = 50 l/min; Ti feed rate, 0.5 g/min; feed gas flow rate, 10 l/min; and measuring position (distance from the nozzle exit), 5 mm.

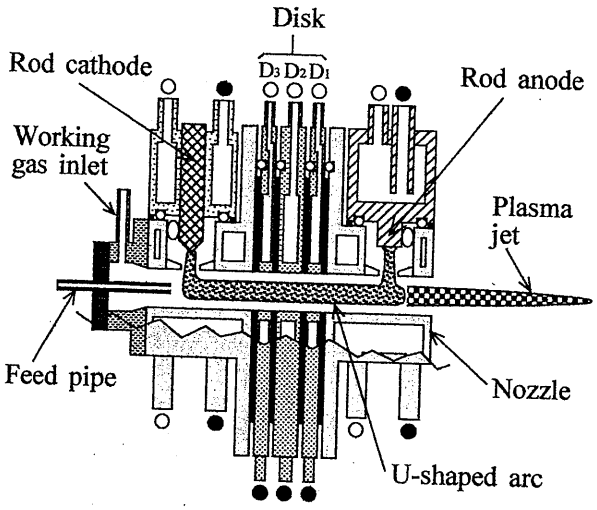

Fig.1 K.Osaki

Reduction rate : 100%

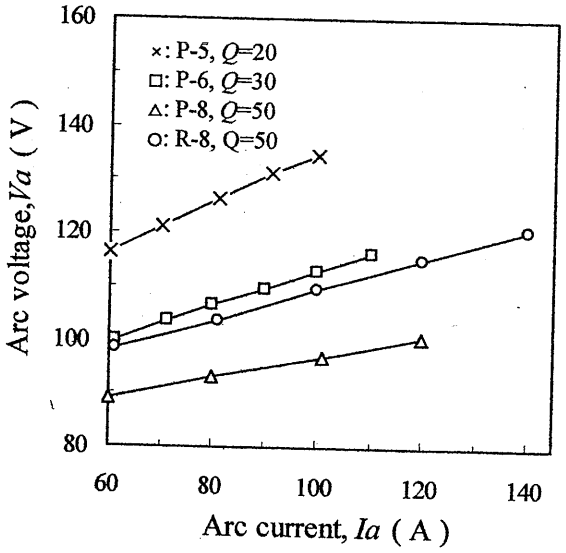

Fig.2 K. Osaki

Reduction rate : 100%

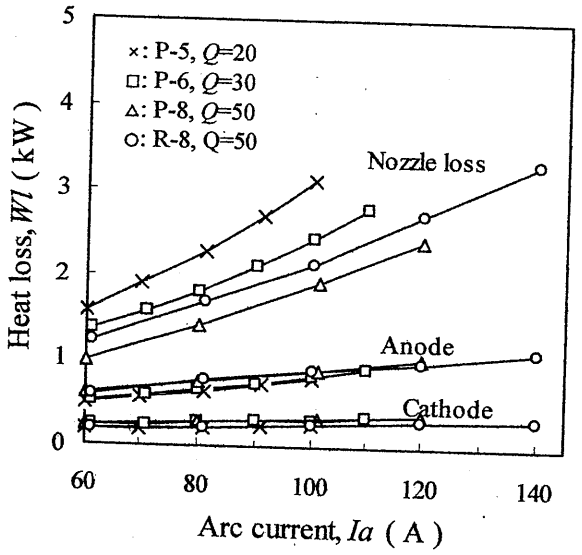

Fig.3 K. Osaki

Reduction rate : 100%

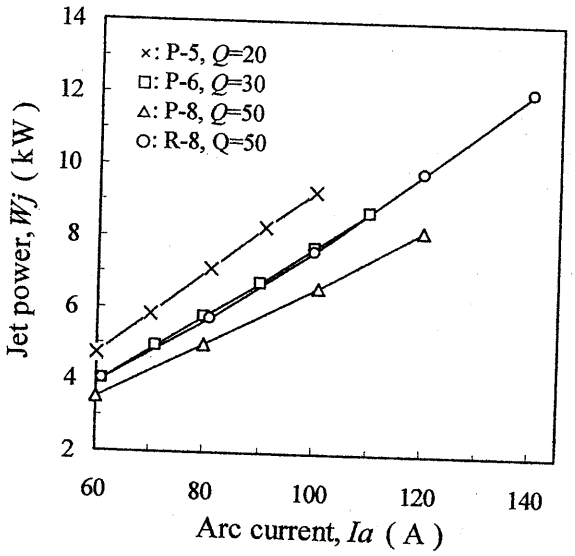

Fig.4 K. Osaki

Reduction rate : 100%

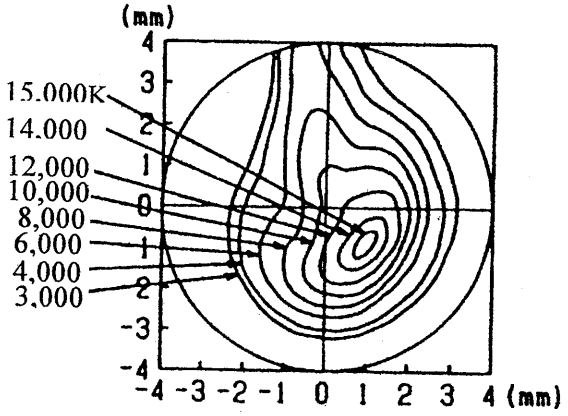

Fig.5 K. Osaki

Reduction rate : 100%

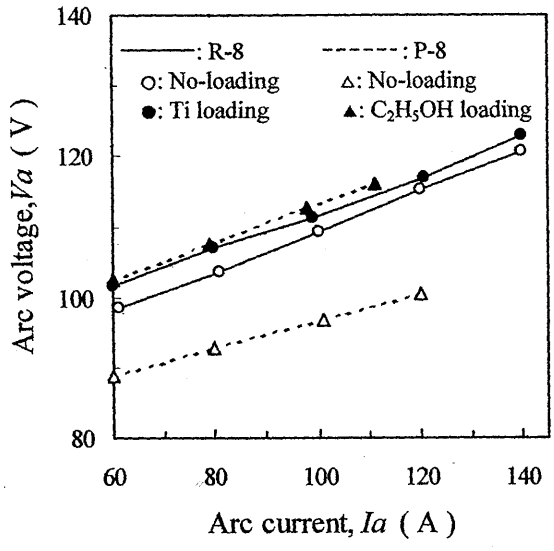

Fig.6 K. Osaki

Reduction rate : 100%

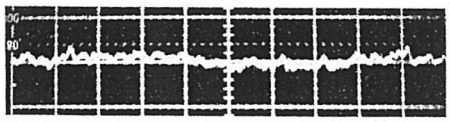

(a) No-loading

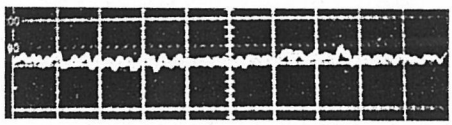

(b) Ti loading, Mf=0.5, Qf=5

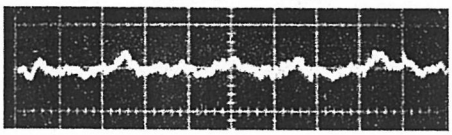

(c) C_2H_5OH loading, Mf=1, Qa=7

Fig.7 K. Osaki

Reduction rate : 100%

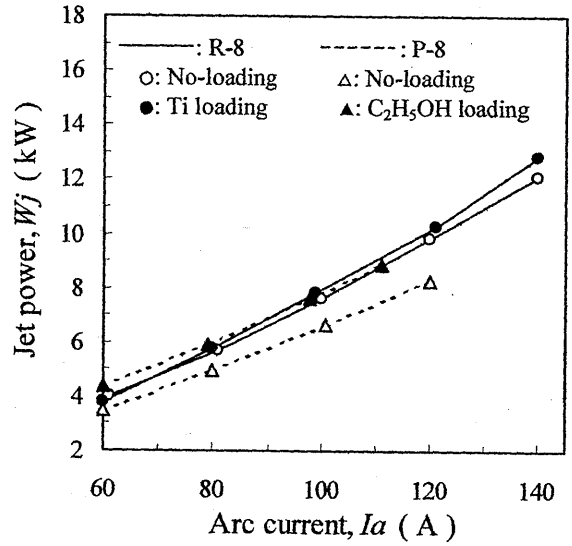

Fig.8 K. Osaki

Reduction rate : 100%

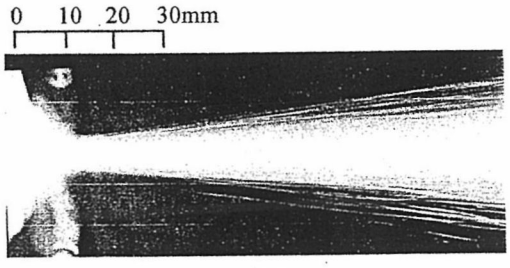

(a) Ti loading, Mf=0.5,Qf=5

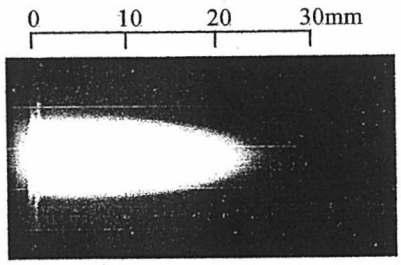

(b) C_2H_5OH loading, Mf=1, Qa=7

Fig.9 K. Osaki

Reduction rate : 100%

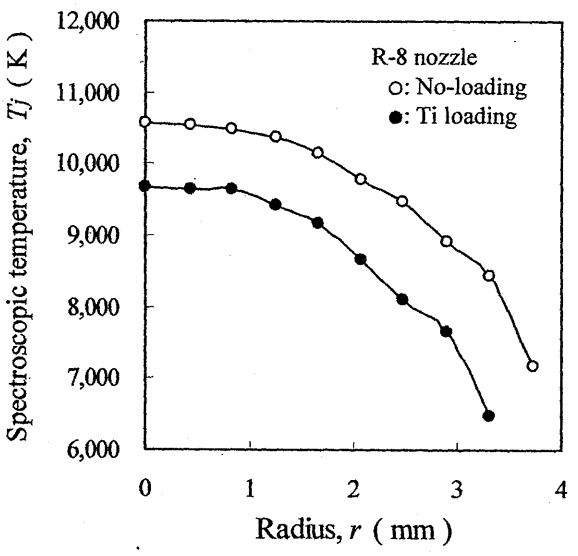

Fig.10 K. Osaki

Reduction rate : 100%